Intravoxel incoherent motion protocol evaluation and data quality in normal and malignant liver tissue and comparison to the literature

Ter Voert, Edwin E G W ; Delso, Gaspar ; Porto, Miguel ; Huellner, Martin ; Veit-Haibach, Patrick

Abstract: OBJECTIVES: Although intravoxel incoherent motion (IVIM) becomes more and more popular, there is currently no clear consensus on the number and distribution of b-values to use. In this work, we (1) tested and evaluated the data quality of a 25-b-value IVIM protocol in patients with malignant liver lesions and normal liver tissue as a standard of reference, (2) calculated an optimal b-value distribution and compared with the standard of reference, and (3) compared the 25-b-value protocol with other proposed protocols in the literature. MATERIALS AND METHODS: Intravoxel incoherent motion imaging with 25 b-values was performed at 3 T in a total of 15 patients with malignant liver lesions. Reference IVIM parameter maps were calculated in tumor and normal liver tissue. With these parameters, optimal IVIM protocols with reduced numbers of b-values were calculated. These optimal IVIM protocols were again applied to calculate new IVIM parameter maps that were compared with the reference parameter maps by calculating mean relative errors. In addition, 35 other IVIM protocols, as found in literature, were compared in a similar way with the 25-b-value protocol serving as a standard of reference. RESULTS: The mean relative error depends on the number of b-values and their distribution. In tumor tissue, the error is higher and more variable than in normal-appearing liver tissue. The largest errors occur in tumor tissue and in the protocols having low numbers of b-values in the IVIM protocols. In the calculated optimal IVIM protocols, the mean relative errors decreased by 40% or more when the number of b-values included increased from 4 to 16. The mean relative errors in the protocols adapted from the literature vary substantially between the various b-value distributions. One optimized 16-b-value protocol, which was found in literature, reduced the average relative error by 80% when compared with 4- and 5-b-value protocols listed in literature. CONCLUSIONS: Including more b-values and applying an optimized b-value distribution significantly reduces errors in the IVIM parameter estimates, thereby increasing its accuracy.This effect is even more pronounced in inhomogeneous tumor compared with that in normal liver tissue. However, when restrictions in acquisition time or patient-related factors apply, a minimum of 16 b-values should be considered for reliable results.

DOI: https://doi.org/10.1097/RLI.0000000000000207

DOI: https://doi.org/10.1097/RLI.0000000000000207

Intravoxel Incoherent Motion Protocol Evaluation and Data Quality in Normal and Malignant Liver Tissue and Comparison to the Literature

Edwin E.G.W. ter Voert, MSc,† Gaspar Delso, PhD,‡ Miguel Porto, BSc,*†*
Martin Huellner, MD,†§ and Patrick Veit-Haibach, MD*†‖*

Objectives: Although intravoxel incoherent motion (IVIM) becomes more and more popular, there is currently no clear consensus on the number and distribution of *b*-values to use. In this work, we (1) tested and evaluated the data quality of a 25–*b*-value IVIM protocol in patients with malignant liver lesions and normal liver tissue as a standard of reference, (2) calculated an optimal *b*-value distribution and compared with the standard of reference, and (3) compared the 25–*b*-value protocol with other proposed protocols in the literature.

Materials and Methods: Intravoxel incoherent motion imaging with 25 *b*-values was performed at 3 T in a total of 15 patients with malignant liver lesions. Reference IVIM parameter maps were calculated in tumor and normal liver tissue. With these parameters, optimal IVIM protocols with reduced numbers of *b*-values were calculated. These optimal IVIM protocols were again applied to calculate new IVIM parameter maps that were compared with the reference parameter maps by calculating mean relative errors. In addition, 35 other IVIM protocols, as found in literature, were compared in a similar way with the 25–*b*-value protocol serving as a standard of reference.

Results: The mean relative error depends on the number of *b*-values and their distribution. In tumor tissue, the error is higher and more variable than in normal-appearing liver tissue. The largest errors occur in tumor tissue and in the protocols having low numbers of *b*-values in the IVIM protocols. In the calculated optimal IVIM protocols, the mean relative errors decreased by 40% or more when the number of *b*-values included increased from 4 to 16. The mean relative errors in the protocols adapted from the literature vary substantially between the various *b*-value distributions. One optimized 16–*b*-value protocol, which was found in literature, reduced the average relative error by 80% when compared with 4– and 5–*b*-value protocols listed in literature.

Conclusions: Including more *b*-values and applying an optimized *b*-value distribution significantly reduces errors in the IVIM parameter estimates, thereby increasing its accuracy.

This effect is even more pronounced in inhomogeneous tumor compared with that in normal liver tissue. However, when restrictions in acquisition time or patient-related factors apply, a minimum of 16 *b*-values should be considered for reliable results.

Key Words: intravoxel incoherent motion, IVIM, perfusion, diffusion, liver, tumor

(*Invest Radiol* 2016;00: 00–00)

Received for publication May 20, 2015; and accepted for publication, after revision, July 24, 2015.

From the *Department of Nuclear Medicine, University Hospital Zurich; †University of Zurich, Zurich, Switzerland; ‡GE Healthcare, Waukesha, WI; Departments of §Neuroradiology, and ‖Diagnostic and Interventional Radiology, University Hospital Zurich, Zurich, Switzerland.

Conflicts of interest and sources of funding: P.V.H. received investigator-initiated study grants from Bayer Healthcare, Siemens Healthcare, and Roche Pharmaceuticals as well as speaker fees from GE Healthcare. G.D. is an employee of GE Healthcare. For the remaining authors, none were declared.

Supplemental digital contents are available for this article. Direct URL citations appear in the printed text and are provided in the HTML and PDF versions of this article on the journal's Web site (www.investigativeradiology.com).

Correspondence to: Edwin E.G.W. ter Voert, MSc, Department of Nuclear Medicine, University Hospital Zurich, Rämistrasse 100, CH-8091 Zurich, Switzerland. E-mail: Edwin.terVoert@usz.ch.

ISSN: 0020-9996/15/0000–0000
DOI: 10.1097/RLI.0000000000000207

Magnetic resonance (MR) diffusion-weighted imaging (DWI) is a very successful and widely used functional imaging protocol providing information about the mobility of water molecules in tissue. By changing the amount of diffusion weighting, the *b*-value, it can be made more sensitive to smaller or larger displacements, such as, for example, in diffusion and perfusion, respectively.

Until recently, the DWI scan protocol was mainly applied to visualize the molecular water diffusion by scanning images with high-diffusion weighting (*b*-values >150 s/mm^2). The diffusion coefficient *D*, representing the true molecular water diffusion, can be obtained by fitting the *b*-values and corresponding measured data to a simple monoexponential diffusion model (Supplemental Digital Content 1, http://links.lww.com/RLI/A221). Because the diffusion is usually restricted in tissue, the diffusion coefficient is also known as the apparent diffusion coefficient.

Where "conventional" DWI is a method to visualize the molecular water diffusion only, intravoxel incoherent motion (IVIM) imaging is a method to visualize both the molecular water diffusion and the information about the microcirculation by using high and low *b*-values. The proposed biexponential IVIM model was described by Le Bihan et al[1,2]:

$$S(b) / S(0) = (1 - f) \times exp(-b \times D) + f \times exp(-b \times [D + D^*]) \quad \text{(Eq. 1)}$$

where f is the fraction of the perfusion component and D^* is the pseudodiffusion coefficient, related to perfusion in the microcirculation.

Intravoxel incoherent motion is becoming more and more popular in clinical research as it provides the additional perfusion information without the need of extensive changes in the MR acquisition protocols.[3–6] The IVIM model is, however, less stable than the monoexponential diffusion model, as it requires the fitting of more variables.

One of the major concerns when implementing an IVIM protocol is the optimal number and distribution of *b*-values. In theory, 4 *b*-values would be sufficient to fit a biexponential function[7]; however, including more *b*-values would make the fit process more robust and enables estimates of parameter uncertainties or quality. This could especially be important for reliable diagnoses and in cases where errors are expected due to, for example, noise, or patient, for example, respiratory and/or cardiac motion.[8,9]

Previously, other studies have investigated potentially optimal *b*-value distributions.[10–14] Lemke et al,[15] for example, performed Monte Carlo simulations to find the optimal *b*-value distributions in tissue with low (brain), medium (kidney), and high (liver) IVIM perfusion. However, in clinical cases, the chosen optimal *b*-value distributions may not perform as one would expect due to, for example, different IVIM parameter ranges in healthy and inhomogeneous tumor tissue.

The aims of this work were (1) to test and evaluate the data quality of a 25–*b*-value IVIM protocol in patients with malignant liver lesions and normal liver tissue as a standard of reference, (2) to calculate an optimal *b*-value distributions and compare to the standard of reference, and (3) to compare the 25–*b*-value protocol with other proposed protocols in the literature concerning data quality.

MATERIALS AND METHODS

Patients

Between September 2012 and January 2014, a total of 15 consecutive patients (mean age, 63 years; range, 33–88 years; 7 women, 8 men) with malignant liver lesions participated in this study. All included patients were referred clinically to our center for PET/CT for either staging or restaging/follow-up of various malignant tumors and volunteered to receive an additional MR imaging (MRI) examination. Exclusion criteria were contraindications to MRI, such as severe claustrophobia, and MRI-incompatible implants, such as cardiac pacemakers, insulin pumps, or neurostimulators. This prospective study was approved by the institutional review board and by the cantonal ethics committee. Signed informed consent was obtained from each patient before the inclusion into this study. Parts of this patient population have been evaluated in other studies in a different context.

Magnetic Resonance Imaging

All MRI examinations were performed on a 3.0-T whole-body MR system (Discovery 750w MR; GE Healthcare, Waukesha, WI) using the body coil for excitation and a posterior and anterior coil array for signal reception.

After conventional T_1- and T_2-weighted imaging, IVIM imaging was performed using a 2-dimensional diffusion-weighted spin-echo single-shot echo-planar imaging sequence covering 8 to 19 slices centered on the lesion of interest. Parallel imaging, array spatial sensitivity encoding technique, was applied to reduce image distortion.

Three different protocols, A, B, and C, were applied, but only 1 in each patient. The acquisition parameters are listed in Table 1. The IVIM acquisitions consisted of 25 *b*-values or diffusion weightings, including $b = 0$ s/mm^2. The 3 orthogonal gradient directions were applied simultaneously (3 in 1). This large set of *b*-values was chosen to have a good representation of all signal values in the interval from $b = 0$ to 800 or 1000 s/mm^2 and still have reasonable imaging times to avoid extensive patient discomfort. Patients continued normal breathing during the acquisition and respiratory gating was applied.

Image Processing

Intravoxel incoherent motion parameter maps were calculated by voxelwise fitting the model of equation 1 to the measured, 25 *b*-values, data using Matlab 2013b (MathWorks, Natick, MA). The applied method is a nonlinear least squares fit using a trust region algorithm.[16] The IVIM parameters *f*, *D*, and *D** were allowed to vary in the reference ranges found in liver and tumors. The boundaries were set to 1.0×10^{-6} and 0.6 for *f*, 0.01×10^{-3} mm^2/s and 3.2×10^{-3} mm^2/s for *D*, and 1×10^{-3} mm^2/s and 500×10^{-3} mm^2/s for *D**. The initial value for *f* was set to 0.2, and the initial value of *D* was set to the estimated diffusion calculated before by fitting the high *b*-values (>100 s/mm^2) to a simple monoexponential diffusion model (Supplemental Digital Content 1, http://links.lww.com/RLI/A221). The initial value of *D** was set to 10 times *D*.

Using PMOD v3.5 (PMOD Technologies, Zurich, Switzerland), the regions of interest (ROIs) were manually drawn on the $b = 0$ s/mm^2 IVIM images around the malignant lesions in the liver on all slices with a visible malignant lesion by a researcher with 5 years of experience. In addition, ROIs with a diameter of approximately 30 mm were drawn in normal-appearing liver tissue, avoiding large vessels and ducts. The ROIs were copied to the IVIM parameter maps, and the voxel values for *f*, *D*, and *D** were extracted to calculate arithmetic means for every ROI. The ROIs were grouped according to tumor or normal tissue type and the minimal; maximal as well as the arithmetic mean and standard deviation were calculated for all IVIM parameters for each group.

Calculation of Optimal *b*-Value Distributions

Reducing the number of diffusion weightings reduces scan time, patient discomfort, and finally acquisition costs. Therefore, new *b*-value distributions with less than 25 *b*-values were calculated to find optimal distributions with less *b*-values and results comparable to the 25–*b*-value distribution. To find these optimal *b*-value distributions, the *b*-values that minimized the error propagation factor ε for the bi-exponential model were selected. The error propagation factor was calculated in a similar way as described by Zhang et al[12] (Supplemental Digital Content 2, http://links.lww.com/RLI/A222). The previously

TABLE 1. IVIM Acquisition Parameters

	Protocol A	Protocol B	Protocol C
TE, ms	69.1–69.3	71.4–71.7	64.2–68.4
TR, ms	4286–6000	4286	3157.9–7500
Flip angle, degrees	90	90	90
No. averages			
$b = 0$ s/mm^2	1	1	1
$b = 10$–200 s/mm^2	4	4	2 or 4
$b = 250$–1000 s/mm^2	1	1	1
Acquisition matrix	128 × 96	160 × 128	160 × 128
Image size	256 × 256	256 × 256	256 × 256
Reconstruction diameter, mm	400	400	400
Pixel size, mm	1.6 × 1.6	1.6 × 1.6	1.6 × 1.6
Slice, mm	8	8	8–10
Parallel imaging	ASSET	ASSET	ASSET
Bandwidth, Hz	1953	1953	1953
Slices	11–14	9–10	8–19
b-values (s/mm^2, n = 25)	0, 15, 30, 45, 60, 75, 90, 110, 130, 150, 170, 185, 250, 300, 350, 400, 450, 500, 550, 600, 650, 700, 750, 800, 1000	0, 13, 25, 38, 50, 63, 75, 88, 100, 113, 125, 138, 150, 163, 175, 188, 200, 300, 400, 500, 600, 700, 800, 900, 1000	0, 10, 20, 30, 40, 50, 60, 70, 80, 90, 100, 110, 120, 130, 140, 150, 160, 170, 180, 190, 200, 350, 500, 650, 800

IVIM indicates intravoxel incoherent motion; ASSET, array spatial sensitivity encoding technique; TE, Echo Time; TR, Repetition Time.

described minimal and maximal *f*, *D*, and *D** values, obtained with the 25–*b*-value distribution, were inserted as the typical parameter ranges for the calculation of the error propagation factor. For the optimization, the parameter ranges for tumor and normal liver tissue were combined.

Because of the long computational time, it is almost impossible to test all possible *b*-value combinations within a reasonable time. To circumvent this problem, the *b*-values were limited to the 25 *b*-values previously defined, and we started with an initial set of 4 *b*-values, as this is the minimum amount of *b*-values needed to fit the biexponential function. This set of initial *b*-values was then extended with *b*-values that continued to minimize ε.

All possible combinations of 4 *b*-values, which included the minimum ($b = 0$ s/mm^2) and the maximum ($b = 800$ or 1000 s/mm^2), were evaluated. The combination that minimized ε was chosen as the optimal 4–*b*-value distribution. The optimal 5–*b*-value distribution was obtained by adding 1 *b*-value to the optimal 4–*b*-value distribution. The added *b*-value should again result in a new combination with minimal ε. This process was repeated until we achieved 22 optimal *b*-value distributions with 4 to 25 *b*-values.

Distributions of *b*-Values in the Literature and Comparison

After calculation of these "optimal" *b*-value distributions, 35 empirically chosen, different *b*-value distributions, as found in literature, were included for comparison. The preferred distributions were IVIM liver tumor protocols covering the range from 4 to 25 *b*-values. In case the preferred distributions were not available in literature, abdominal IVIM protocols with a *b*-value range between 0 and 1000 s/mm^2 were preferably selected. For comparison, several IVIM protocols intended for other tissues were added (Supplemental Digital Content 3, http://links.lww.com/RLI/A223).[7,10,11,15,17–31] The literature-based *b*-values were mapped to the nearest *b*-values available in the measured standard of reference 25–*b*-value data sets.

The work by Lemke et al[15] was also included as many groups refer to their article and use their recommendations for *b*-value distributions. They list 3 types of tissue comparable with low (brain), medium (kidney), and high (liver) IVIM perfusion, and the *b*-value range (0-1000 s/mm^2) is comparable with other (liver) studies included in this work. Lemke presented multiple *b*-value distributions, some of them having duplicate *b*-values in 1 distribution. Only the unique *b*-values and *b*-values near the measured 25 *b*-values were selected in this research to avoid mapping problems. This evaluation has been taken as one of the literature references since it is one of the very few studies trying to find the optimal *b*-value distribution and evaluating these distributions, with up to 16 *b*-values, in healthy volunteers.

Error Calculations

The calculated optimal *b*-value distributions, the mapped *b*-value distributions from literature, and their corresponding measured signals were used to calculate new IVIM parameter maps by fitting the model of Equation 1 to the data, in the same way as described before with the 25–*b*-value distribution. The *f*, *D*, and *D** voxel values in the ROIs were again extracted and compared with the values that were previously calculated using the 25–*b*-value distribution. The relative mean absolute error γ in each ROI was then calculated with:

$$\gamma x = \frac{\frac{1}{N}\sum_{i=1}^{N}\left|X_i - X_{i,ref}\right|}{X_{ref}} \qquad \text{(Eq. 2)}$$

where X is 1 of the 3 parameters *f*, *D*, or *D**, N is the number of voxels in the ROI, X_i is the fitted result in a voxel in the ROI, $X_{i,ref}$ is the fitted result in the corresponding voxel in the 25–*b*-value based reference, and X_{ref} is the arithmetic mean of all $X_{i,ref}$ in the ROI. Voxels with $f_{ref} < 10^{-4}$, $D^*_{ref} < 10^{-5}$ mm^2/s, or $D_{ref} < 10^{-6}$ mm^2/s were excluded.

The calculated relative errors were grouped together according to tissue type and number of *b*-values or literature protocols, and arithmetic means and standard deviations were calculated for each group.

RESULTS

In protocol group A, 4 patients were scanned. One patient had no or very small tumors (<15 mm diameter) and was excluded for the lesion analysis. One patient was included after radiotherapy and had 2 metastases from melanoma that were both included. The 2 other patients had lesions from breast cancer and a metastatic melanoma without treatment. In protocol group B, 5 patients were scanned. One patient had 2 very large colon metastases in the liver and was excluded for the normal liver tissue analysis as no large enough region could be identified as normal liver. Two patients had no or very small tumors (<15 mm diameter), and 1 patient had motion artifacts; all were excluded for the lesion analysis. One patient had 2 metastases from primary bronchial lung carcinoma, and both were included. In protocol group C, 6 patients were scanned. Two patients had no or very small tumors (<15 mm diameter), and 1 patient had motion artifacts; all were excluded for the lesion analysis. The other 3 patients had metastases from primary cholangiocarcinoma, colon cancer, and pancreatic cancer. Of these, the first patient was scanned before therapy, the latter 2 after chemotherapy.

Overall, 14 ROIs (median size, 277 voxels; range, 277–807 voxels) of normal liver tissue and 11 ROIs (median size, 422 voxels; range, 50–4624 voxels) within malignant liver lesions were evaluated.

Examples of the IVIM parameter maps are shown in Figure 1. Differences in the perfusion fraction (*f*), the pseudodiffusion (*D**), and the diffusion (*D*) maps, when calculated with 4–, 9–, and 25–*b*-value distributions, can clearly be appreciated.

The minimal, maximal, arithmetic mean, and standard deviation for *f*, *D*, and *D** in tumor and normal liver tissue, calculated with the 25–*b*-value data sets, are listed in Table 2.

Calculation of Optimal *b*-Value Distributions

Optimal parameter distributions for the 3 protocols A, B, and C were calculated by inserting the previously evaluated minimal and maximal values for *f*, *D*, and *D** (Table 2) in the cost function of Zhang et al. The resulting *b*-value distributions are shown in Table 3.

These optimal parameter distributions were tested by calculating the relative errors γ, and the results are shown in Figure 2. It shows the mean relative error γ for all the calculated optimal *b*-value distributions with 4 to 25 *b*-values. In both, normal liver tissue and tumor tissue, a clear trend of decreasing mean relative error can be observed when the number of *b*-values increases. The mean relative error in tumor tissue is somewhat higher and more variable than in normal-appearing liver tissue. The largest errors occur in the pseudodiffusion, *D**, especially in tumor tissue and in the range where there are low numbers of *b*-values in the distributions. The mean relative errors for 4 *b*-values are 0.51 for *f*, 2.08 for *D**, and 0.36 for *D* in tumor and 0.40 for *f*, 0.98 for *D**, and 0.45 for *D* in the normal liver tissue. The mean relative errors for 16 *b*-values are 0.29 for *f*, 0.52 for *D**, and 0.18 for *D* in tumor and 0.19 for *f*, 0.33 for *D**, and 0.14 for *D* in the normal liver tissue. The mean relative errors decreased by 40% or more when the number of *b*-values included increased from 4 to 16.

Distributions of *b*-Values in Literature and Comparison

The mean relative errors for the modified and mapped *b*-value distributions by Lemke et al,[15] shown in Figure 3, display a similar decreasing trend as the calculated optimal *b*-value distributions when more *b*-values are included. The mean relative errors for 4 *b*-values are 0.42 for *f*, 3.02 for *D**, and 0.26 for *D* in tumor and 0.41 for *f*, 2.19 for *D**, and 0.44 for *D* in the normal liver tissue. The mean relative errors for 16 *b*-values are 0.18 for *f*, 0.47 for *D**, and 0.17 for *D* in tumor

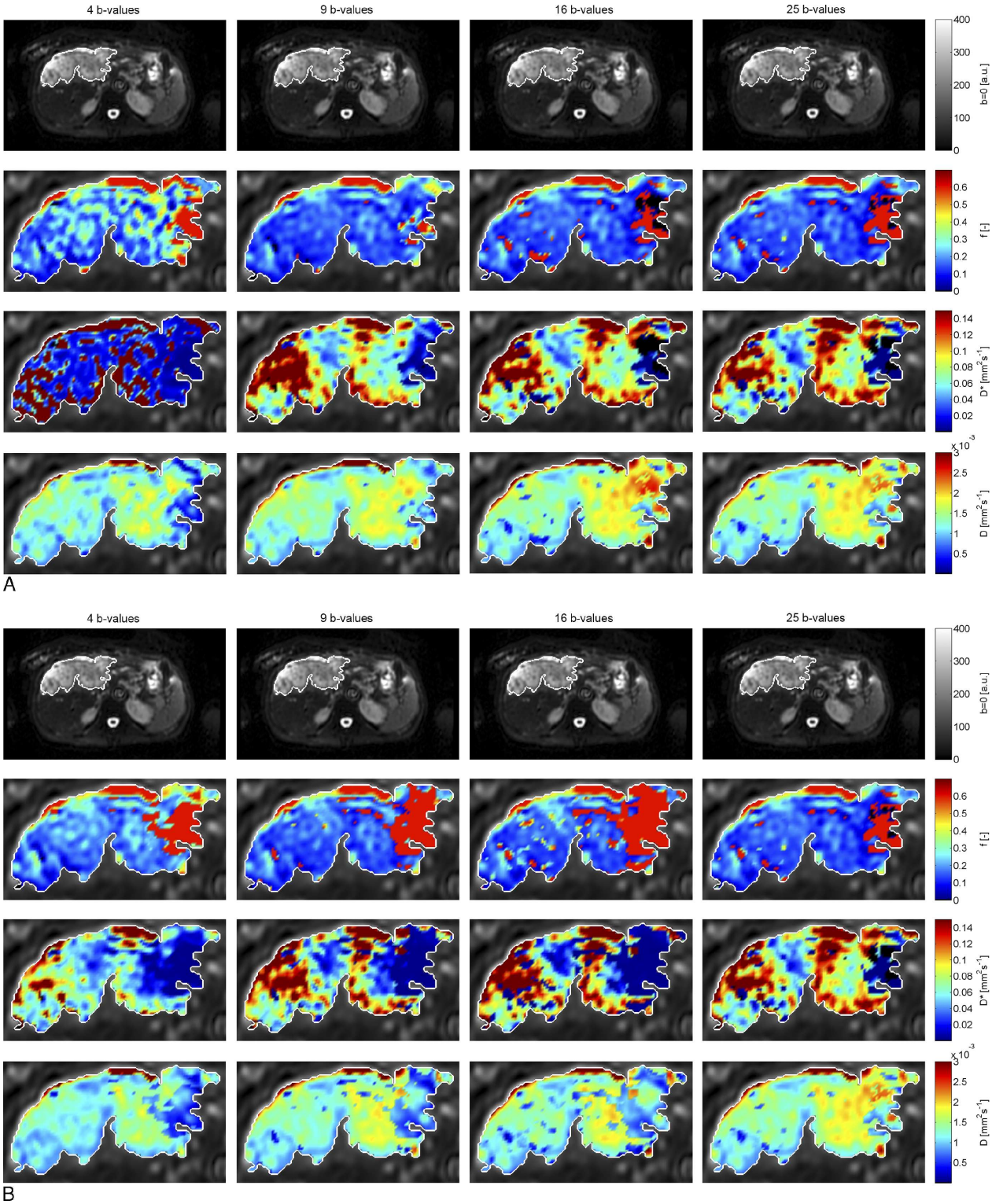

FIGURE 1. Example of IVIM parameter maps calculated with (A) 4– (far left column; Döpfert et al[7]), 9 (left column; Cohen et al[10]), 16– (right column; Wurnig et al[17]), and 25– (right column; reference) *b*-value distributions; (B) optimal 4– (far left column), 9– (left column), 16– (right column), and 25– (far right column) *b*-value distributions. The top row shows an axial unweighted ($b = 0$ s/mm^2) DWI image with a liver lesion. The liver lesion ROI is indicated by a white line in all images. The second row shows the perfusion fraction (*f*) maps, the third row shows the pseudodiffusion (*D**) maps, and the bottom row shows the diffusion (*D*) maps. The map images only show the area containing the liver lesion ROI. The maps clearly show differences when calculations are performed with less *b*-values, and they also show that the tissue inside the ROI is inhomogeneous. The optimal 4– and 9–*b*-value distributions perform better than the corresponding literature distributions. However, in this liver lesion, the 16–*b*-value distribution by Wurnig et al performs better than the optimal 16–*b*-value distribution. Figure 1 can be viewed online in color at www.investigativeradiology.com.

TABLE 2. The Calculated IVIM Parameters *f*, *D*, and *D** Using 25 *b*-Values

	Tumor			Normal Liver		
	***f*, %**	***D*, $\times 10^{-3}$ mm^2/s**	***D**, $\times 10^{-3}$ mm^2/s**	***f*, %**	***D*, $\times 10^{-3}$ mm^2/s**	***D**, $\times 10^{-3}$ mm^2/s**
Minimum*	13	0.46	5.26	19	0.43	24.6
Maximum*	58	1.98	123.0	43	1.13	278.8
Mean (SD)*	32 (13)	1.24 (0.45)	55.0 (36.4)	30 (6.8)	0.83 (0.18)	124.4 (84.5)

*The values are minimum, maximum, and mean (SD) of the mean ROI voxel values.
IVIM indicates intravoxel incoherent motion.

and 0.14 for *f*, 0.22 for *D**, and 0.15 for *D* in the normal liver tissue. This means that the relative errors decreased by 35% or more when the number of *b*-values included increased from 4 to 16.

The mean relative errors in the protocols adapted from the literature (Fig. 4) vary substantially between the various *b*-value distributions. The mapped 11–*b*-value distribution by Leporq et al[21] performs clearly better than the mapped 9–*b*-value distribution by Klauss et al,[26] whereas the 6 *b*-values between 100 and 800 s/mm^2 are the same in both cases. The differences are mainly found in the lower *b*-value range where the former has 2 more *b*-values. The protocols by Hiepe et al[19] and Ichikawa et al[20] have a relative higher number of low *b*-values (<100 s/mm^2). These protocols also have lower errors in the pseudoperfusion *D**.[19,20]

The 16–*b*-value distribution by Wurnig et al,[17] which is taking into account the findings of Lemke et al,[15] performs best of the *b*-value distributions found in literature with mean relative errors of 0.18 for *f*, 0.61 for *D**, and 0.16 for *D* in tumor and 0.16 for *f*, 0.28 for *D**, and 0.16 for *D* in normal liver tissue. It reduces the average error by 80% when compared with the 4– and 5–*b*-value protocols. Figure 4 also shows that, on average, the mean relative error is larger in liver tumor tissue compared with that in normal liver tissue for *f* and *D**, whereas for *D*, the mean relative error is larger in normal liver tissue.

DISCUSSION

Although IVIM becomes more and more popular, there is currently no clear consensus on the number and distribution of *b*-values to use. In this study, we acquired a rather extensive 25–*b*-value IVIM protocol as a standard of reference to evaluate the data quality of other IVIM protocols having less *b*-values. The evaluation was performed for normal liver tissue and for malignant liver lesions. We showed that IVIM data quality improves significantly when the number of *b*-values included in the protocol is increased, making IVIM modeling more robust.

The clinical role of IVIM is yet not completely defined, but there is certainly great potential in clinical routine applications. Because there is proof that multiparametric imaging can improve diagnostic accuracy,[32,33] there is large interest to explore the possibilities of already available techniques, for example, diffusion sequences. Because IVIM is not only able to measure diffusion but also the microperfusion, it could provide additional information concerning the tumor's oxygenation status before therapy. This is important in scenarios where, for example, antiangiogenic therapy is planned or, vice versa, tumor perfusion is first therapeutically enhanced to ensure adequate delivery of chemotherapy to the tumor. However, before such therapy decisions can be based on imaging-derived parameters, it has to be ensured that data quality is sufficient, measurements are highly reliable, and patient-based influences are kept to a minimum.

Early IVIM studies usually evaluated a limited amount of up to 8 *b*-values and are likely chosen empirically. Having a limited number of *b*-values increases the risk of higher errors as, for example, 1 outlier already could have a large effect on the model fitting procedure and thus on the resulting IVIM parameters. Conversely, obtaining more than the minimal required 4 *b*-values for IVIM requires more scan time, and too extensive MR protocols may increase patient discomfort, which could again lead to patient motion and thus acquisition errors. Therefore, the clinically acceptable imaging time for IVIM was limited to 5 to 6 minutes in our study. In these 5 to 6 minutes, we were able to acquire a 25–*b*-value IVIM reference scan protocol. With these 25 *b*-values, we have significantly more data points available for the fitting procedure than the average 4– to 16–*b*-value IVIM protocols listed in literature. This allows us to use it as a reference in the comparison with other IVIM protocols.

Scanning an extensive 25–*b*-value IVIM protocol is not always desirable or even possible. For homogeneous tissue, when the expected IVIM parameter ranges are small and known beforehand, one could calculate and apply an optimal IVIM protocol with a reduced number of *b*-values and still would have sufficient data quality. A number of studies were dedicated on finding optimal *b*-value distributions: for example, Dyvorne et al[14] evaluated optimized *b*-value distributions in the liver for subjects enrolled in a liver fibrosis study. Although this study was also performed in the liver, the tissue properties (perfusion and diffusion) in tumors are different compared with that in (malignant) liver lesions. Jambor et al[13] determined the optimal *b*-value distribution for healthy prostate tissue with *b*-values up to 2000 s/mm^2. However, for prostate imaging, usually higher *b*-values are applied.

Zhang et al[12] optimized the *b*-value sampling for a biexponential DWI model of the kidney, and Lemke et al[15] optimized the *b*-value distributions in tissue for low (brain), medium (kidney), and high (liver) IVIM perfusion. The studies by Jambor et al, Zhang et al, and Lemke et al were, however, validated in healthy volunteers. Tumorous tissue is known to be more inhomogeneous based on distorted cell conglomerates and partially inadequate blood supply and is therefore partially composed of necrotic tissue. Thus, the microperfusion and diffusion characteristics are significantly different compared with that in normal

TABLE 3. Optimal *b*-Value Distributions for Protocol A, B, and C

	Initial *b*-Values, s/mm^2	Added *b*-Values, s/mm^2
Protocol A	0, 15, 170, 1000	800, 45, 750, 700, 60, 650, 250, 75, 600, 90, 550, 500, 30, 110, 450, 130, 400, 150, 350, 185, 300
Protocol B	0, 13, 175, 1000	800, 50, 900, 700, 63, 600, 75, 500, 163, 38, 400, 88, 300, 25, 100, 113, 125, 200, 138, 188, 150
Protocol C	0, 20, 150, 800	650, 50, 10, 500, 60, 350, 70, 40, 200, 80, 30, 190, 90, 180, 100, 170, 110, 120, 160, 130, 140

For the optimization, the parameter ranges for tumor and normal liver tissue (Table 2) were combined.

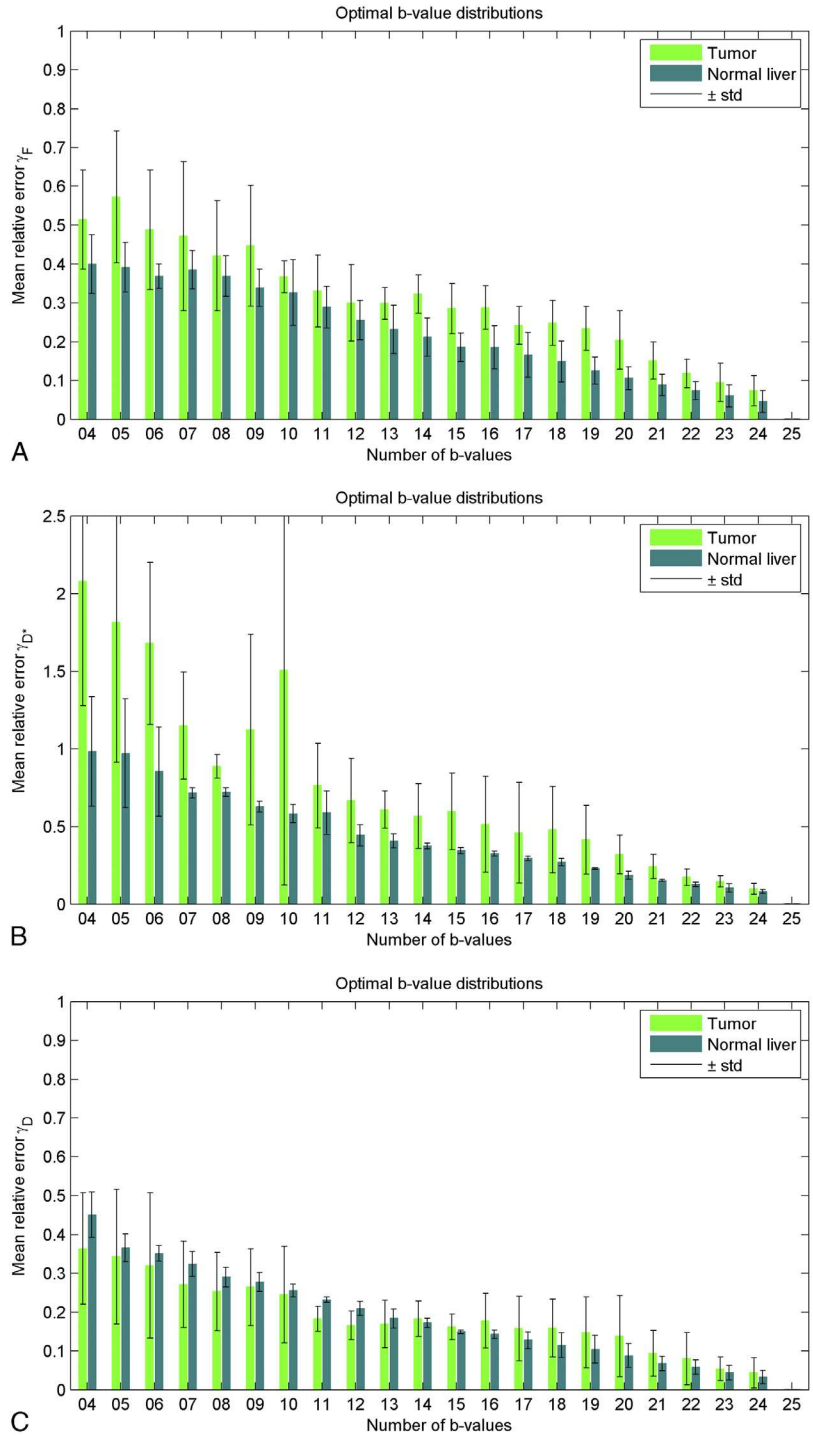

FIGURE 2. The mean relative errors γ in the IVIM parameters for the optimal *b*-value distributions calculated with a cost function by Zang et al[12]: (A) the error in the perfusion fraction, *f*; (B) the error in the pseudodiffusion, *D**; (C) the error in the diffusion, *D*. From left to right in each figure, an increasing number of *b*-values, indicated by the number next to the horizontal axis. On the right side of every graph is the reference with 25 *b*-values, which should have a mean relative error of zero. The light green bars indicate the errors in the tumor tissue, the dark green bars indicate the error in the normal-appearing liver tissue, and std is the standard deviation of the relative error. Figure 2 can be viewed online in color at www.investigativeradiology.com.

tissue. Consequently, the expected IVIM parameters and their ranges are different in pathologic lesions, and the presented optimal distributions may no longer be optimal for these cases and errors may increase.

Because the diffusion coefficient is more related to the high *b*-values, tissue with a high diffusion coefficient could need more *b*-values in this region and/or more signal averages to increase signal to noise ratio and measured accuracy for a more reliable fit, although the error in the diffusion estimation is usually relatively low compared with that in the pseudodiffusion constant, which is approximately 2 to 3 times higher (Figs. 2, 3). The pseudodiffusion constant is more related to the low

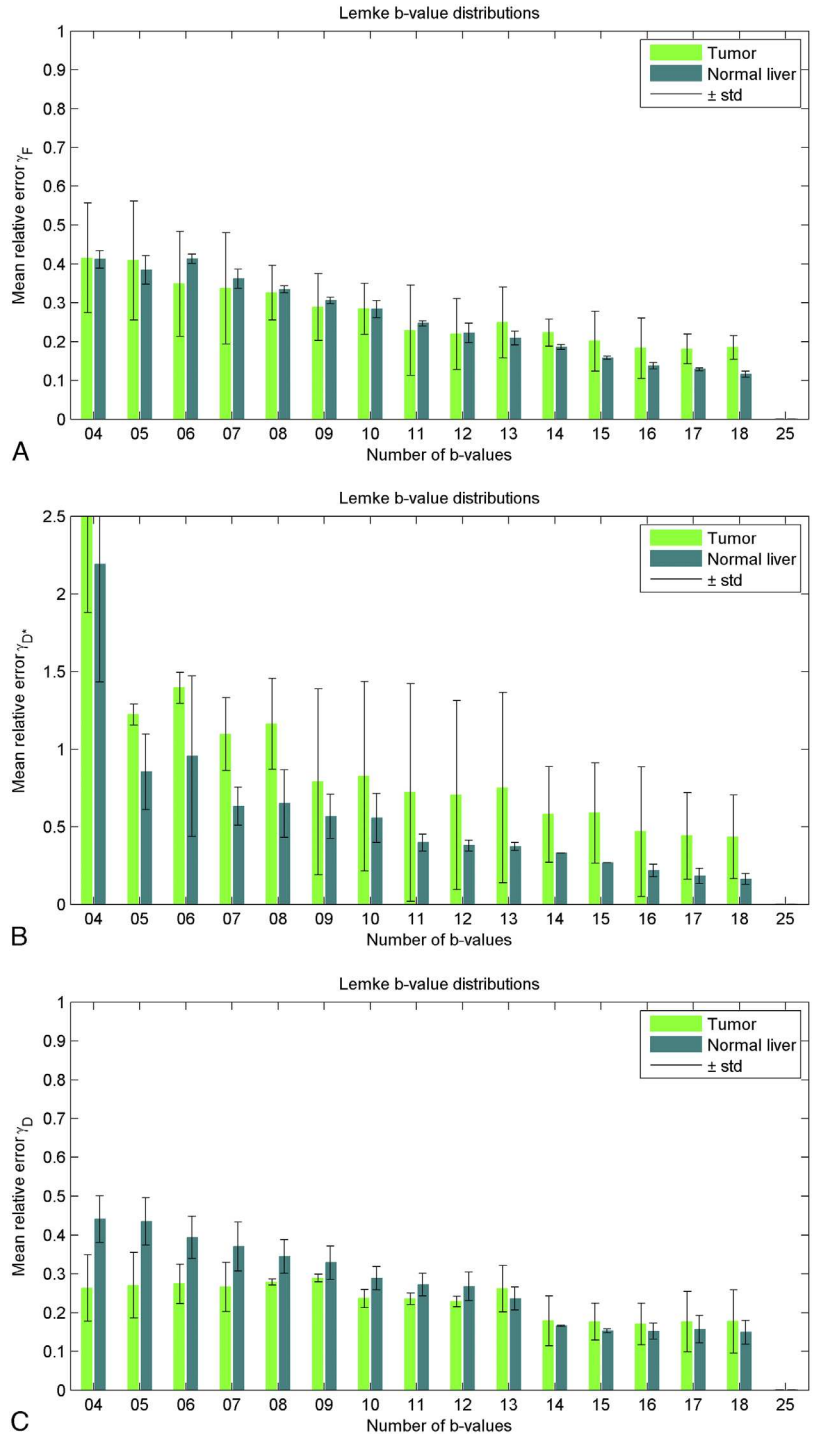

FIGURE 3. The mean relative errors γ in the IVIM parameters for the *b*-value distributions by Lemke et al[15]: (A) the error in the perfusion fraction, *f*; (B) the error in the pseudodiffusion, *D**; (C) the error in the diffusion, *D*. From left to right in each figure, an increasing number of *b*-values indicated by the number next to the horizontal axis. On the right side of every graph is the reference with 25 *b*-values, which should have a mean relative error of zero. The light green bars indicate the errors in the tumor tissue, the dark green bars indicate the error in the normal-appearing liver tissue, and std is the standard deviation of the relative error. Figure 3 can be viewed online in color at www.investigativeradiology.com.

b-values. This corresponds to the steep part in the measured signal versus *b*-value graph (Supplemental Digital Content 4, http://links.lww.com/RLI/A224). This part is more difficult to fit reliably, especially in tissue with a high perfusion factor. Protocols with a relative higher number of low *b*-values, such as that of Ichikawa et al and Hiepe et al, have a lower relative error for the pseudodiffusion *D** (Fig. 4).[19,20] More parameter considerations can be found in Supplemental Digital Content 5, http://links.lww.com/RLI/A226.

Overall, the diffusion parameter *D* has the smallest relative error, followed by the perfusion fraction *f* and the pseudodiffusion *D**. The

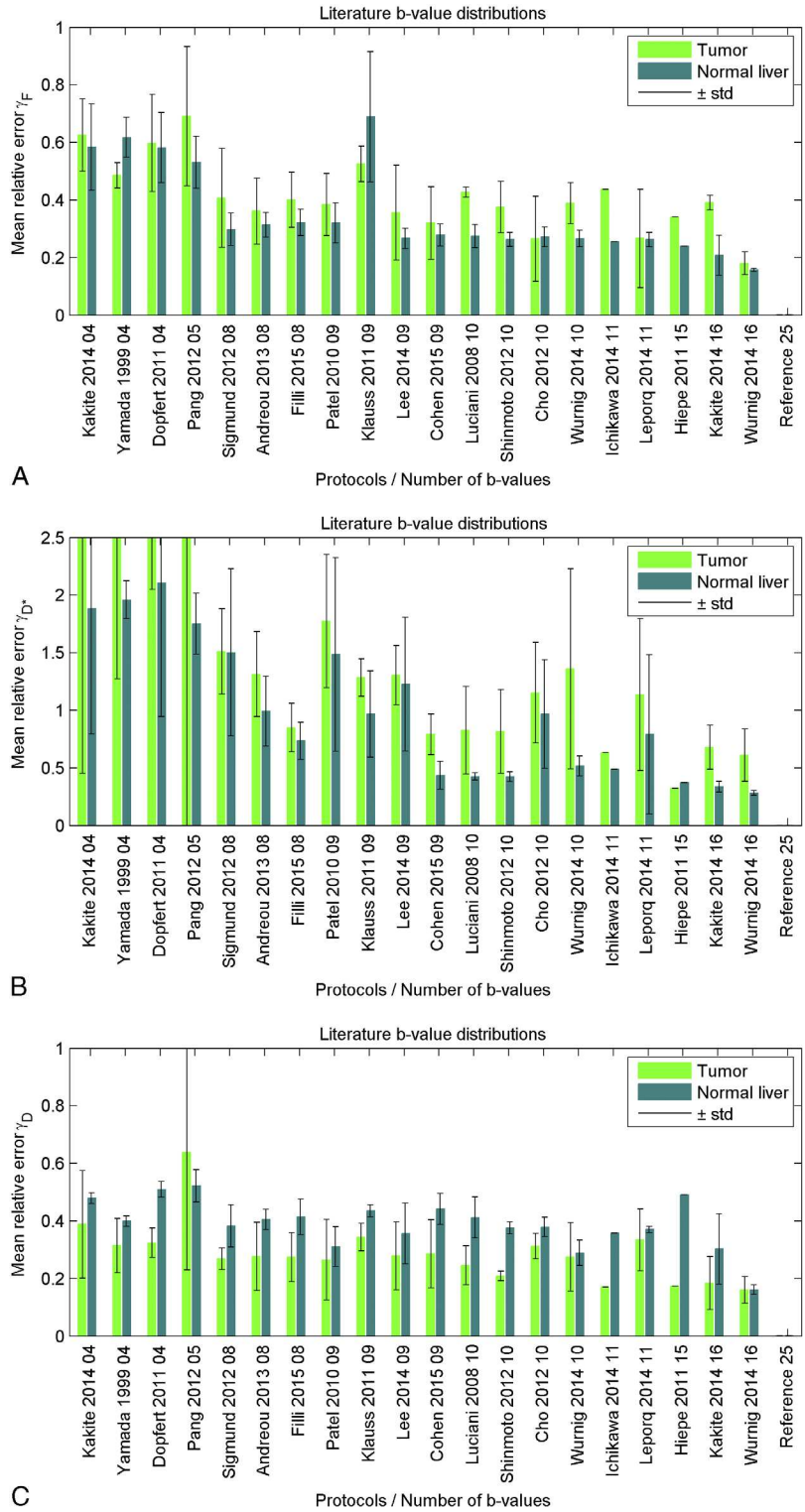

FIGURE 4. The mean relative errors γ in the IVIM parameters for the *b*-value distributions found in literature (see also Supplemental Digital Content 3, http://links.lww.com/RLI/A223): (A) the error in the perfusion fraction, *f*; (B) the error in the pseudodiffusion, *D**; (C) the error in the diffusion, *D*. From left to right in each figure, an increasing number of *b*-values, indicated by the number next to the horizontal axis. On the right side of every graph is the reference with 25 *b*-values, which should have a mean relative error of zero. The light green bars indicate the errors in the tumor tissue, the dark green bars indicate the error in the normal-appearing liver tissue, and std is the standard deviation of the relative error. The figure does not show a quality measure for the work performed by the listed researchers. Included protocols may not have been intended for IVIM on malignant liver lesions and are only added for comparison. Figure 4 can be viewed online in color at www.investigativeradiology.com.

latter is usually worst with the largest relative error. Similar results are reported in literature for different scanning and fitting methods and tissues.[12,14,15,21,34,35]

The largest gain in error reduction is in the range when moving from 4 to 11 *b*-values (for example, see Figs. 2, 3). Therefore, we would consider 11 *b*-values an absolute minimum. These findings are similar to previous work by Lemke et al and Jambor et al in healthy liver, kidney, and spleen.[13,15] Dyvorne et al[14] on the other hand recommended a minimum of 4 *b*-values for their liver fibrosis study. Their *D** reproducibility was, however, significantly worse compared with that of other studies. The authors claim that this could be related to the wider parameter range they allowed in their study. If the expected IVIM parameter range is very small, an optimized protocol could reduce the number of *b*-values even further. However, in tumor tissue, a larger parameter range is expected, and therefore more *b*-values need to be included.

With 16 *b*-values, the error is reduced even further (see also Figs. 2, 3) while the acquisition time is still reasonable. With the optimal calculated *b*-value distributions we, for example, showed that the mean relative error in normal liver tissue is less than 0.2 with 16 *b*-values (Fig. 2). Therefore, we would recommend 16 *b*-values.

However, when analyzing inhomogeneous tumor tissue with the same reduced amount of (optimized) *b*-values, the mean relative error increased to 0.5. The results in Figure 3 show that (the mapped versions of) the distributions proposed by Lemke et al are comparable to our optimized distributions and also have an increased error in tumor tissue compared with that in normal liver tissue. Therefore, when analyzing (inhomogeneous) tumor tissue, or multiple organs, large differences in IVIM parameters and reduced data quality have to be expected. These wide ranges in expected IVIM parameters make it hard to find optimal *b*-value distributions. In these cases, it recommends scanning as many *b*-values as time permits.

Although not all protocols available in the literature comparison were intended for IVIM or liver tumor analysis (Supplemental Digital Content 3, http://links.lww.com/RLI/A223), the results, presented in Figure 4, show that a suboptimal choice of *b*-values could lead to large errors. For example, the mapped protocols by Patel et al, Klauss et al, Lee et al, and Cohen et al all have 9 *b*-values, but the latter has the smallest mean relative errors. It even performs better than the mapped 11–*b*-value protocol by Leporq et al. The mapped 16–*b*-value distribution by Wurnig et al[17] performs best of the 20 literature cases. It is taking into account the findings of Lemke et al,[15] meaning that a useful *b*-value distribution should have more *b*-values in the 0 to 50 s/mm^2 range and less in the midrange of 450 to 800 s/mm^2 in a distribution up to 1000 s/mm^2.

As mentioned previously, motion could play an important role in abdominal imaging. The larger relative error in tumor tissue compared with that in normal-appearing tissue could also be partially explained by motion and partial volume. Respiratory motion and cardiac and aortic pulsations cause the position of the tumor to change during scanning.[36] As a result, surrounding liver tissue could move in and out of the tumor ROIs and, in addition, because tumor tissue is often less homogeneous than liver tissue, motion in a tumor ROI could have a larger effect than motion inside a normal liver ROI when comparing IVIM parameter maps. Respiratory and cardiac gating could circumvent this problem, but it would roughly double the total IVIM acquisition time. Increasing the number of signal averages could improve the results, but often only by blurring the motion artifact. A better solution could be scanning duplicate *b*-values and rejecting data points that are affected by motion during postprocessing. This way, the increased scan time could lead to an increase in signal to noise, of course depending on the amount of data points that are not rejected. Instead of rejecting data points, one could also perform motion correction. As the high *b*-value images have only a limited amount of signal and are therefore difficult to register, one could scan in a different way, for example, alternating low *b*-value with high *b*-value scans.[37]

Our study has some limitations. Repeatedly adding *b*-values to a set of optimal *b*-values does not necessarily lead to the best *b*-value set with the lowest cost. Testing all possible *b*-value combinations would be better; however, such computations are almost impossible due to the very high number of possible combinations. In addition, the mapping of the *b*-values, as found in literature, to the nearest *b*-value in our 25–*b*-value IVIM protocol could have an effect on the mean relative error, although the effect is expected to be minimal.

CONCLUSIONS

Including more *b*-values and applying an optimized *b*-value distribution significantly reduces errors in the IVIM parameter estimates, thereby increasing its accuracy.

This effect is even more pronounced in inhomogeneous tumor compared with that in normal liver tissue. However, when restrictions in acquisition time or patient-related factors apply, a minimum of 16 *b*-values should be considered for reliable results.

REFERENCES

1. Le Bihan D, Breton E, Lallemand D, et al. Separation of diffusion and perfusion in intravoxel incoherent motion MR imaging. *Radiology*. 1988;168:497–505.
2. Le Bihan D, Breton E, Lallemand D, et al. MR imaging of intravoxel incoherent motions: application to diffusion and perfusion in neurologic disorders. *Radiology*. 1986;161:401–407.
3. Ebrahimi B, Rihal N, Woollard JR, et al. Assessment of renal artery stenosis using intravoxel incoherent motion diffusion-weighted magnetic resonance imaging analysis. *Invest Radiol*. 2014;49:640–646.
4. Gaing B, Sigmund EE, Huang WC, et al. Subtype differentiation of renal tumors using voxel-based histogram analysis of intravoxel incoherent motion parameters. *Invest Radiol*. 2015;50:144–152.
5. Hwang EJ, Lee JM, Yoon JH, et al. Intravoxel incoherent motion diffusion-weighted imaging of pancreatic neuroendocrine tumors: prediction of the histologic grade using pure diffusion coefficient and tumor size. *Invest Radiol*. 2014; 49:396–402.
6. Iima M, Yano K, Kataoka M, et al. Quantitative non-Gaussian diffusion and intravoxel incoherent motion magnetic resonance imaging: differentiation of malignant and benign breast lesions. *Invest Radiol*. 2015;50:205–211.
7. Döpfert J, Lemke A, Weidner A, et al. Investigation of prostate cancer using diffusion-weighted intravoxel incoherent motion imaging. *Magn Reson Imaging*. 2011;29:1053–1058.
8. Kwee TC, Takahara T, Koh DM, et al. Comparison and reproducibility of ADC measurements in breathhold, respiratory triggered, and free-breathing diffusion-weighted MR imaging of the liver. *J Magn Reson Imaging*. 2008;28:1141–1148.
9. Kwee TC, Takahara T, Niwa T, et al. Influence of cardiac motion on diffusion-weighted magnetic resonance imaging of the liver. *MAGMA*. 2009;22:319–325.
10. Cohen AD, Schieke MC, Hohenwalter MD, et al. The effect of low *b*-values on the intravoxel incoherent motion derived pseudodiffusion parameter in liver. *Magn Reson Med*. 2014;73:306–311.
11. Pang Y, Turkbey B, Bernardo M, et al. Intravoxel incoherent motion MR imaging for prostate cancer: an evaluation of perfusion fraction and diffusion coefficient derived from different *b*-value combinations. *Magn Reson Med*. 2013;69: 553–562.
12. Zhang JL, Sigmund EE, Rusinek H, et al. Optimization of *b*-value sampling for diffusion-weighted imaging of the kidney. *Magn Reson Med*. 2012;67:89–97.
13. Jambor I, Merisaari H, Aronen HJ, et al. Optimization of *b*-value distribution for biexponential diffusion-weighted MR imaging of normal prostate. *J Magn Reson Imaging*. 2014;39:1213–1222.
14. Dyvorne H, Jajamovich G, Kakite S, et al. Intravoxel incoherent motion diffusion imaging of the liver: optimal *b*-value subsampling and impact on parameter precision and reproducibility. *Eur J Radiol*. 2014;83:2109–2113.
15. Lemke A, Stieltjes B, Schad LR, et al. Toward an optimal distribution of b values for intravoxel incoherent motion imaging. *Magn Reson Imaging*. 2011;29: 766–776.
16. Yuan YX. Recent advances in trust region algorithms. *Mathematical Programming*. 2015;151:249–281.
17. Wurnig MC, Donati OF, Ulbrich E, et al. Systematic analysis of the intravoxel incoherent motion threshold separating perfusion and diffusion effects: proposal of a standardized algorithm. *Magn Reson Med*. 2014. [Epub ahead of print].
18. Kakite S, Dyvorne H, Besa C, et al. Hepatocellular carcinoma: short-term reproducibility of apparent diffusion coefficient and intravoxel incoherent motion parameters at 3.0T. *J Magn Reson Imaging*. 2015;41:149–156.

19. Hiepe P, Reichenbach JR. Functional muscle MRI in human calf muscle using IVIM. Proceedings of the 19th Annual Meeting ISMRM, Montreal, QC, Canada, 2011; 2013.
20. Ichikawa S, Motosugi U, Morisaka H, et al. MRI-based staging of hepatic fibrosis: comparison of intravoxel incoherent motion diffusion-weighted imaging with magnetic resonance elastography. *J Magn Reson Imaging*. 2015;42:204–210.
21. Leporq B, Saint-Jalmes H, Rabrait C, et al. Optimization of intra-voxel incoherent motion imaging at 3.0 Tesla for fast liver examination. *J Magn Reson Imaging*. 2015;41:1209–1217.
22. Cho GY, Kim S, Jensen JH, et al. A versatile flow phantom for intravoxel incoherent motion MRI. *Magn Reson Med*. 2012;67:1710–1720.
23. Luciani A, Vignaud A, Cavet M, et al. Liver cirrhosis: intravoxel incoherent motion MR imaging—pilot study. *Radiology*. 2008;249:891–899.
24. Shinmoto H, Tamura C, Soga S, et al. An intravoxel incoherent motion diffusion-weighted imaging study of prostate cancer. *AJR Am J Roentgenol*. 2012;199: W496–W500.
25. Lee Y, Lee SS, Kim N, et al. Intravoxel incoherent motion diffusion-weighted MR imaging of the liver: effect of triggering methods on regional variability and measurement repeatability of quantitative parameters. *Radiology*. 2015;274:405–415.
26. Klauss M, Lemke A, Grünberg K, et al. Intravoxel incoherent motion MRI for the differentiation between mass forming chronic pancreatitis and pancreatic carcinoma. *Invest Radiol*. 2011;46:57–63.
27. Patel J, Sigmund EE, Rusinek H, et al. Diagnosis of cirrhosis with intravoxel incoherent motion diffusion MRI and dynamic contrast-enhanced MRI alone and in combination: preliminary experience. *J Magn Reson Imaging*. 2010;31:589–600.
28. Filli L, Wurnig MC, Luechinger R, et al. Whole-body intravoxel incoherent motion imaging. *Eur Radiol*. 2015;25:2049–2058.
29. Andreou A, Koh DM, Collins DJ, et al. Measurement reproducibility of perfusion fraction and pseudodiffusion coefficient derived by intravoxel incoherent motion diffusion-weighted MR imaging in normal liver and metastases. *Eur Radiol*. 2013;23:428–434.
30. Sigmund EE, Vivier PH, Sui D, et al. Intravoxel incoherent motion and diffusion-tensor imaging in renal tissue under hydration and furosemide flow challenges. *Radiology*. 2012;263:758–769.
31. Yamada I, Aung W, Himeno Y, et al. Diffusion coefficients in abdominal organs and hepatic lesions: evaluation with intravoxel incoherent motion echo-planar MR imaging. *Radiology*. 1999;210:617–623.
32. Scheenen TW, Rosenkrantz AB, Haider MA, et al. Multiparametric magnetic resonance imaging in prostate cancer management: current status and future perspectives. *Invest Radiol*. 2015;50:594–600.
33. Heijmen L, ter Voert EE, Oyen WJ, et al. Multimodality imaging to predict response to systemic treatment in patients with advanced colorectal cancer. *PLoS One*. 2015;10:e0120823.
34. Suo S, Lin N, Wang H, et al. Intravoxel incoherent motion diffusion-weighted MR imaging of breast cancer at 3.0 tesla: Comparison of different curve-fitting methods. *J Magn Reson Imaging*. 2015;42:362–370.
35. Cho GY, Moy L, Zhang JL, et al. Comparison of fitting methods and *b*-value sampling strategies for intravoxel incoherent motion in breast cancer. *Magn Reson Med*. 2014.
36. Kitamura K, Shirato H, Seppenwoolde Y, et al. Tumor location, cirrhosis, and surgical history contribute to tumor movement in the liver, as measured during stereotactic irradiation using a real-time tumor-tracking radiotherapy system. *Int J Radiat Oncol Biol Phys*. 2003;56:221–228.
37. Mazaheri Y, Do RK, Shukla-Dave A, et al. Motion correction of multi-*b*-value diffusion-weighted imaging in the liver. *Acad Radiol*. 2012;19:1573–1580.
38. Zhou IY, Gao DS, Chow AM, et al. Effect of diffusion time on liver DWI: an experimental study of normal and fibrotic livers. *Magn Reson Med*. 2014;72:1389–1396.
39. de Bazelaire CM, Duhamel GD, Rofsky NM, et al. MR imaging relaxation times of abdominal and pelvic tissues measured in vivo at 3.0 T: preliminary results. *Radiology*. 2004;230:652–659.
40. Sanches-Gonzalez J. How to Identify and Avoid Artifacts on DWI. *Diffusion MRI Outside the Brain—A Case-Based Review and Clinical Applications*. Berlin, Heidelberg: Springer; 2012:17–31.